Planetary and Space Science 121 (2016) 53–59

Contents lists available at ScienceDirect

Planetary and Space Science

journal homepage: www.elsevier.com/locate/pss

Raman spectroscopy: Caution when interpreting organic carbon from oxidising environments

Connor Brolly*, John Parnell, Stephen Bowden

Department of Geology & Petroleum Geology, University of Aberdeen, Aberdeen, UK

ARTICLE INFO

Article history:
Received 1 May 2015
Received in revised form
7 December 2015
Accepted 9 December 2015
Available online 25 December 2015

Keywords:
Raman spectroscopy
Oxidation
Organic carbon
Oxidised carbon
ExoMars

ABSTRACT

Oxidation on Mars is primarily caused by the high influx of cosmic and solar radiation which interacts with the Martian surface. The evidence of this can be seen in the ubiquitous red colouration of the Martian sediment. This radiation will destroy most signals of life in the top few metres of the Martian surface. If organic carbon (one of the building blocks of life) is present within the accessible Martian sediments, it is very likely that it will have experienced some oxidation. ESA's ExoMars mission set to fly in 2018, has on board a miniaturised Raman spectrometer. As Raman spectroscopy is sensitive to carbonaceous material and will be primarily used to characterise organics, it is essential that the effect oxidation has on the Raman carbon signal is assessed. Oxidised carbonaceous shales were analysed using Raman spectroscopy to assess this issue. Results show that haematite has a band which occurs in the same frequency as the carbon D band, which cannot be distinguished from each other. This can lead to a misidentification of the carbon D band and a misinterpretation of the carbon order. Consequently, caution must be taken when applying Raman spectroscopy for organic carbon analysis in oxidised terrestrial and extraterrestrial environments, including on Mars.

1. Introduction

1.1. Oxidation on Mars

Due to an extremely thin atmosphere and lack of a global magnetic field, galactic cosmic rays (GCRs) and solar energy particles (SEPs) penetrate the Martian surface (e.g. Dartnell et al., 2007). This irradiation reacts with H_2O molecules and can generate HO. radicals which can produce peroxides or other oxidising species through reactions with elements in the Martian soil (Benner et al., 2000; ten Kate et al., 2005).

The evidence of this oxidation can be seen in the ubiquitous red colouration of the Martian sediment, which is conferred from oxidised iron in the form of haematite, goethite or maghemite (Morris et al., 1997, 2000). High concentrations of oxidised iron have been observed by MER Opportunity at Meridiani Planum (Hurowitz et al., 2010) and MSL Curiosity (Blake et al., 2013) at Gale Crater, and more widely at Gale Crater by CRISM (Fraeman et al., 2013). This radiation will likely destroy any signatures of life such as biomarkers, over a thousand million years (Pavlov et al., 2013), as well as cells or spores which lie in the top few metres of the Martian soil (ten Kate et al., 2005; Schuerger et al., 2006). Therefore the effect radiation has on the preservation and detection of life is extremely important, in the search for life there.

Carbon in its reduced form is an important target for the search for life as it can represent past life or an energy stock for existing life (Parnell et al., 2013). Finding well preserved organic matter is also the primary target for the ESA ExoMars rover landing site, due to fly in 2018. If organic matter is present within accessible Martian sediments, it is very likely that it will have experienced some oxidation (Hartman and McKay, 1995). Therefore determining the effect of oxidation or oxidative weathering has on the carbon signal is fundamental to the search for life on Mars. The ExoMars rover will have capabilities to potentially drill beneath this oxidised zone (Vago et al., 2006), where life signatures may still be preserved (Griffiths et al., 2006, Zent, 1998). However assessing the potential issues associated with organic detection in an oxidising environment would give useful insight into instrument capabilities, in preparation for this mission.

1.2. Raman spectroscopy for Mars

The popularity of Raman spectroscopy for sample characterisation has dramatically increased in the last 20 years, due to its expanding range of applications across many disciplines (Pérez and Martinez-Frias, 2006). It is a non-destructive technique, which is important for remote missions, as conserving samples for analyses by other instruments is essential for maximising data

* Corresponding author. Tel.: +44 1224 273433; fax: +44 1224272785.
E-mail address: c.brolly@abdn.ac.uk (C. Brolly).

http://dx.doi.org/10.1016/j.pss.2015.12.008

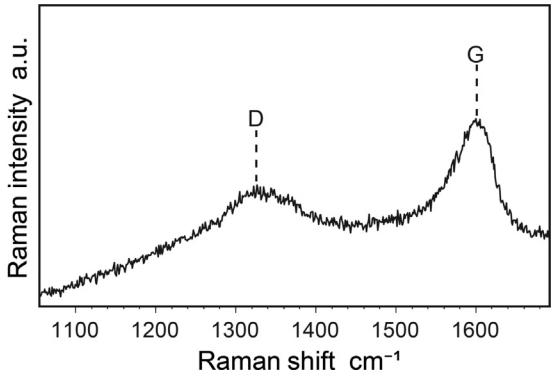

Fig. 1. Raman spectra of kerogen showing the disordered (D) and graphitic (G) bands. *x*-axis (Raman shift) is in reciprocal centimetres (cm^{-1}), and the *y*-axis (Raman intensity) is in arbitrary units (a.u.). G band represents in plane vibrations of aromatic carbons in the graphitic structure. D band attributed to structural defects. The relationship of these two bands gives information on order and thermal maturity.

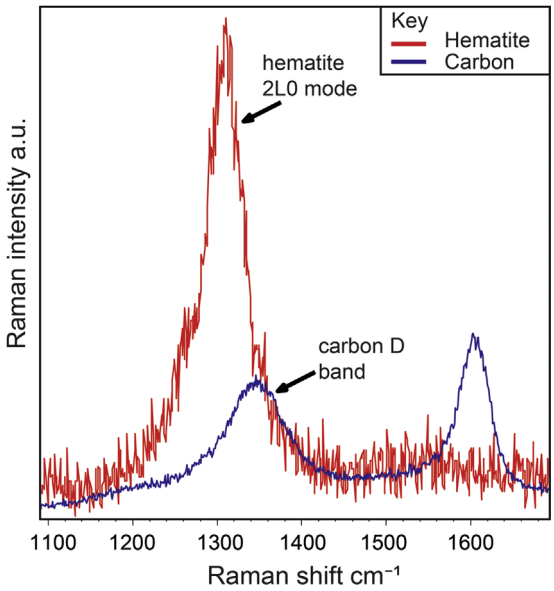

Fig. 2. Raman spectra of haematite (red) and carbon (blue). *x*-axis (Raman shift) is in reciprocal centimetres (cm^{-1}), and the *y*-axis (Raman intensity) is in arbitrary units (a.u.). The haematite 2LO mode is broad and intense and overlaps the carbon D band. (For interpretation of the references to color in this figure legend, the reader is referred to the web version of this article.)

extracted from each sample. It is sensitive to biomolecules and their components such as aromatic compounds, photo-synthetic and photo-protective pigments (Ellery and Wynn-Williams, 2003). It has a wavelength range which covers most vibrational modes including carbonates, silicates and sulphates (i.e., most rock-forming minerals) and metal oxides, therefore it can also be used for petrographic analysis (Haskin et al., 1997; Wang et al., 1998). A micro laser Raman spectrometer is planned as part of the payload instrumentation for the 2018 European Space Agency ExoMars mission (Vago et al., 2006). Experiments were carried out with this mission in mind, but can equally be applied to future surface landers.

1.3. Raman spectroscopy of organic carbon

Raman spectroscopy of carbonaceous material occurs at two wavelength bands. The first, known as 'first order bands' occur between 1100–1800 cm^{-1} (Tuinstra and Koenig, 1970). The spectra of organic material in this order is characterised by two main bands; the graphitic (G) band, which occurs at ~1600 cm^{-1}; and the disordered (D) band, which occurs ~1350 cm^{-1}, as shown in Fig. 1.

The G band represents in-plane vibrations of aromatic carbons in the graphitic structure (Beyssac et al., 2002). In highly ordered material this band shifts down to 1580 cm^{-1}, and displays an additional band at 1620 cm^{-1}, called disordered 2 (D2) (Beyssac et al., 2002). In poorly ordered carbon it occurs as a broad band at 1600 cm^{-1} in which the D2 shoulder cannot be resolved (Beyssac et al., 2002). The D band is intense and broad in poorly ordered carbon. In more ordered carbon, the band area reduces with stiffening of the aromatic planes and is attributed to in-plane defects e.g., heteroatoms or structural defects (Beyssac et al., 2002). The second order bands, occur between 2700–3100 cm^{-1}, and displays a number of bands which relate overtone and combination scattering (Wopenka and Pasteris, 1993).

To quantify the maturity of sp^2 carbonaceous material, common parameters are used and are outlined by Beyssac et al. (2002, 2003). The intensity ratio ($R1$) is $D_{intensity}/ G_{intensity}$, and in general the $R1$ value increases with disorder. The area ratio ($R2$) is the $D1_{area} /(G_{area}+D1_{area}+D2_{area})$, and decreases with increasing metamorphic grade. In poorly ordered spectrum the D2 cannot be distinguished from the G band, therefore the $D2$ band will be disregarded in the $R2$ equation.

1.4. Raman spectroscopy of haematite and carbon

Work by Marshall and Olcott Marshall (2013) discusses the Raman spectrum of sp^2 carbonaceous material mixed with haematite. The haematite 2LO mode, which is attributed to defects in the haematite lattice, occurs in the frequency of the carbon D band (A1g mode). Fig. 2 shows the Raman spectra of haematite and sp^2 carbonaceous first order spectrum from an Ordovician carbonaceous mudstone. The haematite 2LO mode occurs around 1320 cm^{-1} and is very intense, and overlaps the carbonaceous spectra. Oxidised spectral bands occurring in the haematite/carbon frequency will be referred to as 'D bands'; however it is a combination of carbon D band plus the haematite 2LO mode.

2. Experimental

2.1. Samples

Carbonaceous mudstone samples which display oxidative weathering were collected from four localities in the British Isles; Carboniferous, Ayrshire, Scotland; Devonian, Caithness; Ordovician, Langness peninsula, Isle of Man. Neoproterozoic, Tanera Beg, Summer Isles (Fig. 3). Samples were collected which displayed a boundary between oxidised and non-oxidised where possible.

The reddening of Carboniferous rocks in Ayrshire, Scotland occurred due to oxidation below the late Carboniferous-early Permian land surface (Mykura, 1960). Analysis of stable haematite grains in Devonian rocks, Caithness shows reddening is dated to Permo-Carboniferous ages (Tarling et al., 1976). Reddening in the Ordovician strata, Isle of Man, occurred after late Carboniferous – Permian uplift (Wang, 1992). Neoproterozoic, Summer Isles has a Permian chemical remnant magnetisation age (Blumstein

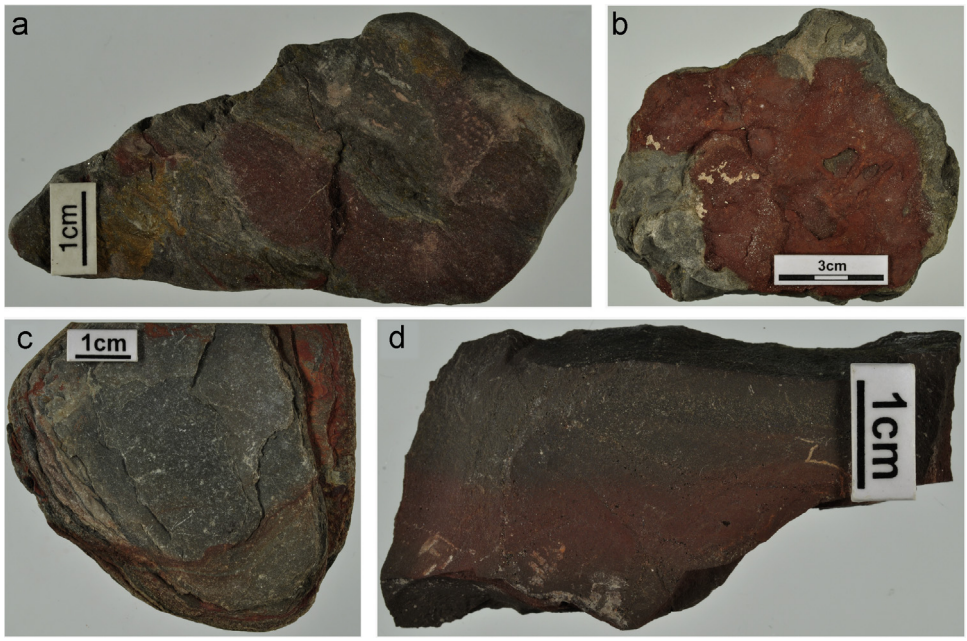

Fig. 3. Reddening of carbonaceous mudstones. (a) Carboniferous, Ayrshire, Scotland (b) Devonian, Caithness (c) Ordovician, Isle of Man (d) Neoproterozoic, Tanera Beg, Summer Isles.

et al., 2005), therefore all samples have been reddened between the Permian and Carboniferous.

The relative amount of haematite in each specimen was determined petrographically. The Devonian sample has the most haematite (c. 20%) as it displays deep, penetrative oxidation through the majority of the sample. The Carboniferous and Neoproterozoic samples contain less haematite (c. 15%) than the Devonian sample but still display reddening which penetrates the surface. The Ordovician sample has the least haematite (c. 10%) as reddening is restricted to bedding surfaces.

2.2. Raman spectroscopy configuration

Raman spectra were obtained using a Renishaw InVia H36031 confocal Raman microscope operating at a wavelength of 514.5 nm green monochromatic laser light, which is similar to the 2018 ExoMars flight instrument wavelength of 532 nm. The laser power was 0.3 mW, avoiding laser-induced heating of the samples and photochemical transformation of Fe-oxides (de Faria et al., 1997). A 50 × objective lens was used giving a laser "footprint" of 1–3 μm (Beyssac et al., 2002), with a static spectral range centred at 1400 cm^{-1}. 8 s exposure time and 8 accumulations were acquired for each spectrum, giving a good signal to noise ratio. The high number of accumulations and exposure time was required to account for increased noise associated with oxidised samples. Spectra were processed using smooth, baseline subtraction and peak fit functions, using Renishaw WiRE 2.0 curve fitting software. Manual baseline subtraction was carried out using cubic spline interpolation function. Peak fitting used a combination of Guassian and Lorentzian algorithms. Due to the order of the carbon, D2 bands were not analysed as they could not be distinguished from the G band (Beyssac et al., 2002). This deconvolution process was repeated 3 times for each spectrum to account for human errors associated with manual baseline subtraction.

2.3. Hydrofluoric acid treatment

Original samples were divided into oxidised and non-oxidised portions. Approximately 3 g of each sample was roughly crushed, by hand, using a pestle and mortar, and treated in 30 ml of hydrofluoric acid. Samples were stirred twice a day for two days to ensure all lithics were dissolved. Samples were then decanted 2 to 3 times a day, until a neutral pH was reached. Excess water was then pipetted off and remaining material was left to dry at room temperature. Samples were then re-analysed using the above settings. Oxidised samples displayed a red colouration after treatment indicating that not all of the iron oxide was removed.

3. Results

3.1. Untreated spectral parameters

Fig. 4 shows representative spectra from whole rock analysis of oxidised and non-oxidised samples. The spectra from non-oxidised Carboniferous and Devonian samples display a broad G band around 1600 cm^{-1}, and a broad, intense D band at 1345 cm^{-1}. The Ordovician and Neoproterozoic spectra show a more intense, narrow G band compared to the Carboniferous and Devonian samples.

The oxidised spectra are markedly different from the non-oxidised spectra. In general the spectra are noisy and have a low count rate (around 500 a.u). One of the most prominent differences is in the D band morphology, which shows an increase in band intensity and width compared to spectra from non-oxidised samples. In oxidised samples the G band also shows a decrease in intensity and width.

The order of the spectra can be quantified using *R*1 and *R*2 parameters (Beyssac et al., 2002), which is shown in Fig. 5. Non-oxidised *R*1 values for the Carboniferous, Devonian, Ordovician and Neoproterozoic are as follows, respectively; 0.5, 0.29, 0.74 and

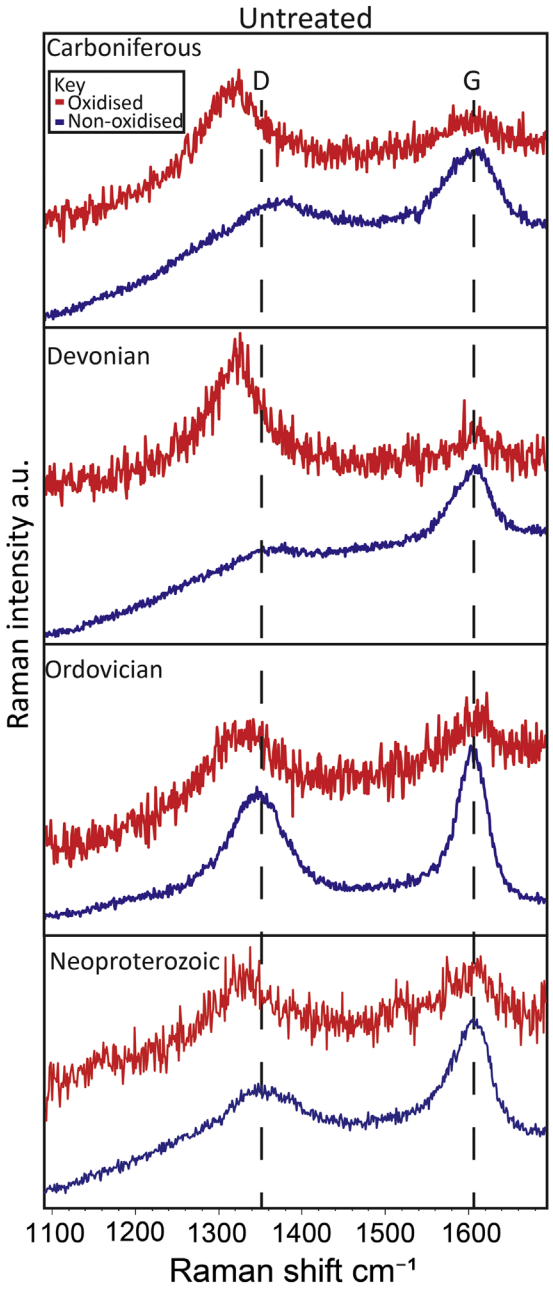

Fig. 4. Representative spectra from whole rock analysis of oxidised and non-oxidised samples. *x*-axis (Raman shift) is in reciprocal centimetres (cm^{-1}), and the *y*-axis (Raman intensity) is in arbitrary units (a.u.). Oxidised spectra are displayed in red; non-oxidised spectra are displayed in blue. D and G band positions are highlighted by dashed line. (For interpretation of the references to color in this figure legend, the reader is referred to the web version of this article.)

0.45. According to Beyssac et al. (2002) *R*1 values decrease with increasing order of organic carbon. However in poorly ordered spectra, the D band is broad and has a low intensity, which gives a lower *R*1 ratio.

Average G band full width at half maximum (FWHM) against G band position is plotted in Fig. 6(a). The Carboniferous non-oxidised sample has an average FWHM of 62.6 cm^{-1} and a band position of 1602 cm^{-1}. The oxidised Carboniferous sample has an average FWHM of 68.7 cm^{-1} and a band position of 1598 cm^{-1}. The Devonian non oxidised sample has an average FWHM of 52.3 cm^{-1} and a band position of 1601 cm^{-1}. The Devonian oxidised sample has an average FWHM of 55.9 cm^{-1} and a band position of 1600 cm^{-1}. The Ordovician non-oxidised sample has an average FWHM of 45.5 cm^{-1} and a band position of 1604 cm^{-1}. The Ordovician oxidised sample has an average FWHM of 49.6 cm^{-1} and a band position of 1604 cm^{-1}. The Neoproterozoic non-oxidised sample has a FWHM of 56.1 cm^{-1} and a band position of 1603 cm^{-1}. The oxidised sample has an average FWHM of 57.1 cm^{-1} and a band position of 1603 cm^{-1}.

Fig. 6(b) shows D band FWHM plotted against D band positions. The D band positions of non-oxidised carboniferous, Devonian, Ordovician and Neoproterozoic samples are as follows, respectively; 1345, 1335, 1346 and 1349 cm^{-1}. Oxidised D band positions of carboniferous, Devonian, Ordovician and Neoproterozoic samples are as follows, respectively; 1321, 1319, 1325 and 1330 cm^{-1}.

3.2. HF treated spectral parameters

To determine if the spectral change is associated with a haematite overprint, the samples were treated with hydrofluoric acid (HF) to concentrate the carbon, but also to remove the haematite. Fig. 7 shows representative spectra of hand crushed, oxidised and non-oxidised samples after hydrofluoric acid treatment.

Oxidised spectra from each sample group have changed spectra morphology after HF demineralisation. The main change is that the D band is no longer broad and intense, and oxidised spectra look very similar to the non-oxidised spectra.

Average G FWHM against G band position is plotted in Fig. 8(a). The Carboniferous non-oxidised sample has an average FWHM of 67.7 cm^{-1} and a band position of 1602 cm^{-1}. The Carboniferous oxidised sample has a FWHM of 67.3 cm^{-1} and a band position of 1600 cm^{-1}. The Devonian non-oxidised sample has an average FWHM of 54.5 cm^{-1} and a band position of 1601 cm^{-1}. The Devonian oxidised sample has an average FWHM of 57.5 cm^{-1} and a band position of 1600 cm^{-1}. The Ordovician non-oxidised sample has an average FWHM of 46.1 cm^{-1} and a band position of 1605 cm^{-1}. The Ordovician oxidised sample has an average FWHM of 49.8 cm^{-1} and a band position of 1605 cm^{-1}. The Neoproterozoic non-oxidised sample has an average FWHM of 56 cm^{-1} and a band position of 1604 cm^{-1}. The Neoproterozoic oxidised sample has an average FWHM of 57.1 cm^{-1} and a band position of 1604 cm^{-1}.

Fig. 8(b) shows D band FWHM plotted against D band positions of HF treated samples. The D band positions of non-oxidised carboniferous, Devonian, Ordovician and Neoproterozoic samples are as follows, respectively; 1351, 1334, 1348 and 1354 cm^{-1}. Oxidised D band positions of carboniferous, Devonian, Ordovician and Neoproterozoic samples are as follows, respectively; 1346, 1340, 1350 and 1355 cm^{-1}.

4. Discussion

4.1. R1 and R2 parameters

Fig. 5(a) is the *R*1 parameter for specimens both oxidised and non-oxidised, and there is a clear difference in *R*1 values. Non-oxidised samples plot around 0.5, and oxidised samples plot between 1 and 3. This increase in *R*1 value (assuming only carbon is present) would suggest that there is a decrease in order between non-oxidised and oxidised spectra. However as the presence of haematite has been established (based on the colour of the material and spectral bands present) it is evident that the increase

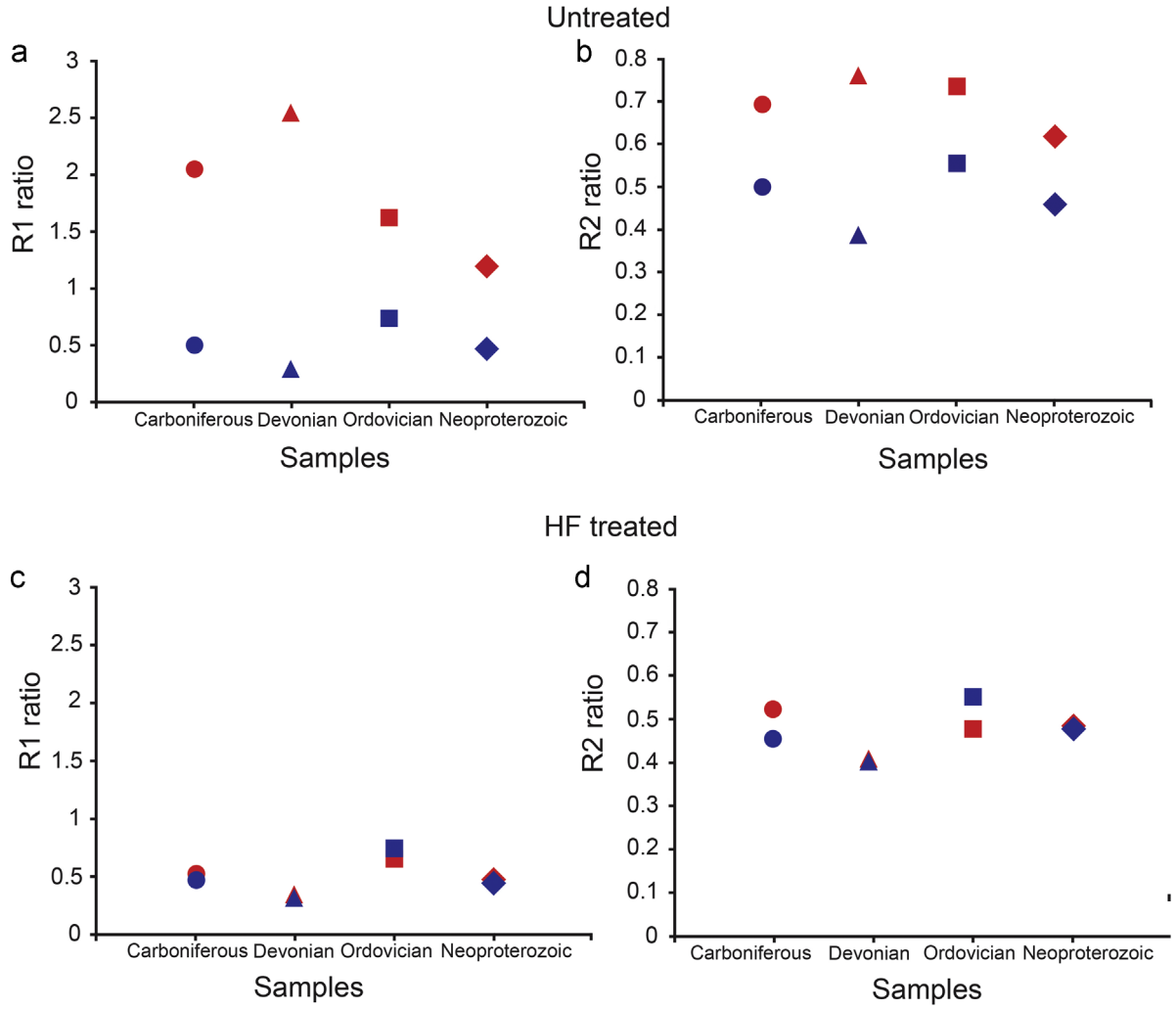

Fig. 5. *R*1 and *R*2 plots for untreated (a, b) and HF treated (c, d) samples. *R*1 (intensity ratio)=*D*/*G*, *R*2 (area ratio)=*D*/(*G*+*D*). Blue points indicate non-oxidised samples. Red points indicate oxidised samples. Each point represents and average of 10 spectra which have been processed each 3 times. (For interpretation of the references to color in this figure legend, the reader is referred to the web version of this article.)

in *R*1 value is due to the haematite 2LO band interfering with the carbon D band.

Fig. 5(b) is the *R*2 parameter for specimens both oxidised and non-oxidised. Oxidised samples plot around 0.7 and non-oxidised plot around 0.6, as an increase in *R*2 ratio relates to a decrease in order. Therefore *R*2 ratios also show the interference from haematite, which overlaps the D carbon band.

After hydrofluoric acid treatment, the difference in *R*1 values between non-oxidised and oxidised samples is reduced. Fig. 5 (c) shows oxidised markers plotting in almost identical positions to non-oxidised markers. This demonstrates that the interfering haematite signal has been removed as a result of HF demineralisation. This shows that haematite interference is causing the change in spectral parameters in the D band frequency, and that the carbon is not affected by HF treatment. No other minerals envisaged to be in the sample e.g., quartz and clays have bands which are as intense, broad and occur in the D band frequency, as the haematite 2LO mode.

Fig. 5(d) is the *R*2 ratio for oxidised and non-oxidised samples after hydrofluoric acid treatment. Oxidised samples have decreased in *R*2 value, plotting close to the non-oxidised samples, indicating the interfering haematite signal has been removed.

4.2. G and D band FWHM vs G and D band position

Fig. 6(a) shows that G band FWHM increases with oxidation and the G band position decreases, in all three sample sets, which is highlighted by the arrows. Conventionally with decreasing order of organic carbon, the G band FWHM increases and the G band position increases. Therefore in oxidised samples there is a converse relationship in the Raman G band parameters. The reason for this relationship is not known, but could be attributed to uncertainties associated with measuring G band parameters in low ordered carbonaceous material outlined by Beyssac et al. (2003).

Fig. 6(b) shows a major difference in D band position between oxidised and non-oxidised samples. Non-oxidised samples plot between 1335 and 1350 cm^{-1}. Oxidised samples plot between 1320 and 1330 cm^{-1}. This is further evidence that the haematite 2LO is overprinting the carbon D band.

Fig. 8(a) shows the G band FWHM against G band positon. The Carboniferous and Devonian oxidised samples show a change in

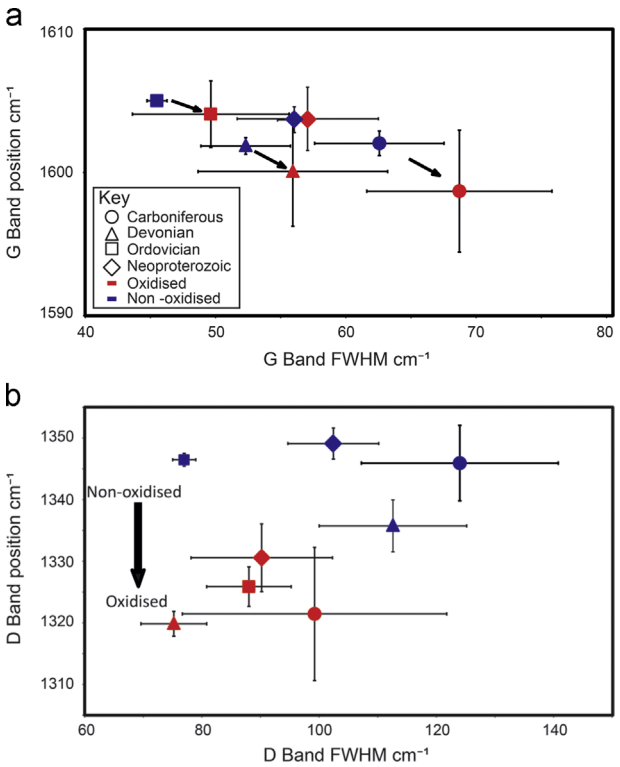

Fig. 6. a) G band FWHM against G band position. Oxidised samples show an increase in FWHM and decrease in band position. Arrows highlight shift in each sample set. (b) D band FWHM against D band position. Oxidised samples shift downward in band position, highlighted by arrow. Shift in D and G band positions associated with haematite interference. Error bars were calculated using one standard deviation.

band position and FWHM, which plot close to the non-oxidised samples.

Fig. 8(b) shows the D band FWHM against D band position. The difference observed in D band position between non-oxidised and oxidised samples is not present in HF treated samples. The oxidised samples show D band positions which plot closer to the carbon D band position. This shows that the majority of the interfering haematite signal has been removed. The slight discrepancy in values is interpreted to be caused by remnant haematite which has not been dissolved by the HF treatment. This is supported by the faint red colouration of samples after HF treatment.

5. Conclusions

Oxidation is prevalent on Mars and must be considered when selecting instrumentation for remote missions there. ESA's ExoMars mission set to fly in 2018, has as part of its payload instrumentation, a miniaturised Raman spectrometer. As Raman is sensitive to carbonaceous material and will be primarily used to characterise organics, it is essential that the effect oxidation has on the Raman carbon signal is assessed. Oxidised shales from the Carboniferous, Devonian and Ordovician were used as analogues to address this question. The morphology of the spectra from oxidised samples are markedly different from non-oxidised. There is a reduction in G band width and intensity, and an increase in D band FWHM and intensity, which is reflected in the *R*1 and *R*2 ratios. Assuming only carbon is present would suggest that oxidation decreases the carbon order. However based on the change in D band position it is clear that the haematite 2LO band at 1320 cm^{-1}, it is overprinting the carbon D band in oxidised samples. This is further supported by hydrofluoric acid treatment which removed the majority of the haematite signal from oxidised samples. This can lead to a misidentification of the carbon D band and a misinterpretation of the carbon order. Therefore, caution must be taken when interpreting Raman spectra of carbon from oxidising environments, including on Mars.

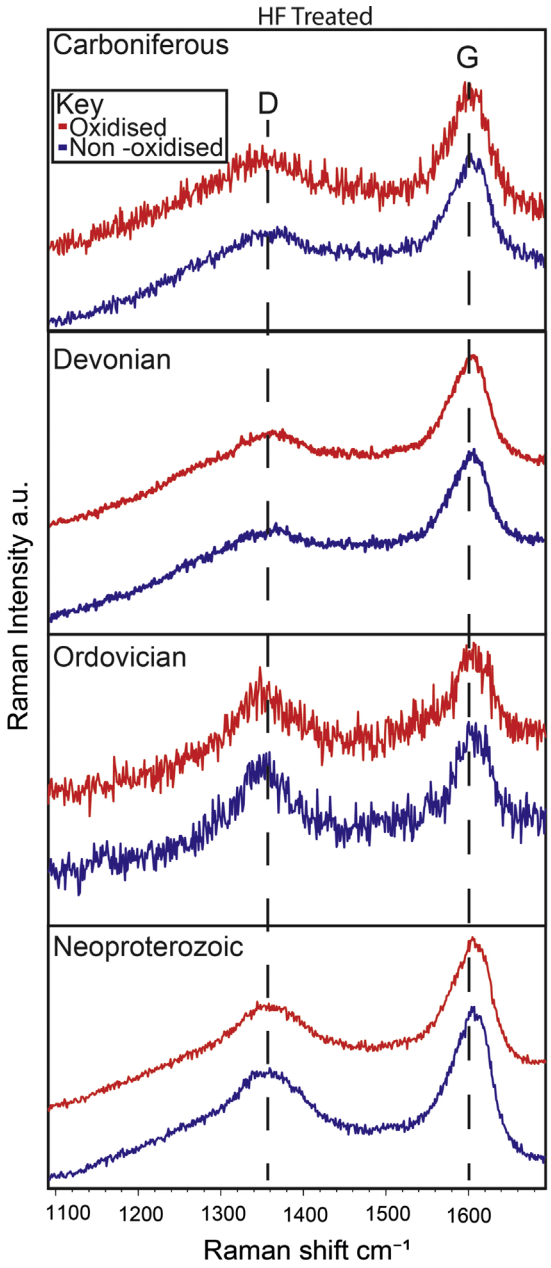

Fig. 7. Representative spectra of hand crushed oxidised and non-oxidised samples after hydrofluoric acid treatment. Oxidised spectra are displayed in red; non-oxidised spectra are displayed in blue. D and G band positions are highlighted by dashed line. Oxidised D band positons are at 1345 cm^{-1}, indicating haematite has been removed by HF treatment. (For interpretation of the references to color in this figure legend, the reader is referred to the web version of this article.)

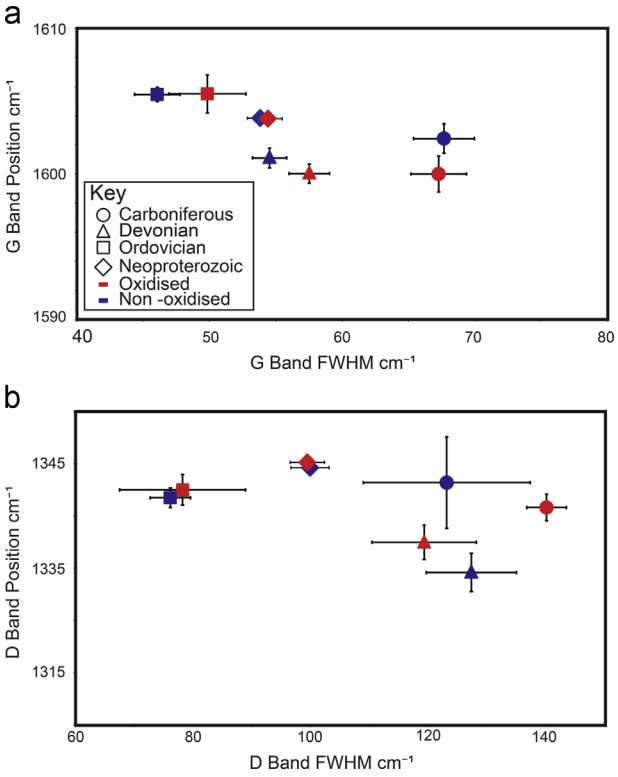

Fig. 8. a) G band FWHM against G band position of hand crushed oxidised and non-oxidised samples after hydrofluoric acid treatment. Oxidised samples are close to their non-oxidised counterparts. (b) D band FWHM against D band position. Oxidised samples show a shift similar Raman band parameters compared to non-oxidised samples indicating that the majority of haematite was removed. Error bars were calculated using one standard deviation of the population.

Acknowledgements

This work was funded by STFC Grant (ST/L001233/1). The University of Aberdeen Raman facility was funded by the BBSRC Grant (BBC5125101). Thanks to Giles Hemmings and Keir Construction for site access for sample collection.

References

Benner, S. a, et al., 2000. The missing organic molecules on Mars. Proc. Natl. Acad. Sci. USA 97 (6), 2425–2430.
Beyssac, O., et al., 2003. On the characterization of disordered and heterogeneous carbonaceous materials by Raman spectroscopy. Spectrochim. Acta-Part A: Mol. Biomol. Spectrosc. 59 (10), 2267–2276.
Beyssac, O., et al., 2002. Raman spectra of carbonaceous material in metasediments: a new geothermometer. J. Metamorph. Geol. 20 (9), 859–871.
Blake, D.F., et al., 2013. Curiosity at Gale crater, Mars: characterization and analysis of the Rocknest sand shadow. Science 341 (6153), 1239505.
Blumstein, R.D., et al., 2005. Multiple fluid migration events along the Moine Thrust Zone, Scotland. J. Geol. Soc. 162 (6), 1031–1045.
Dartnell, L.R., et al., 2007. Martian sub-surface ionising radiation: biosignatures and geology. Biogeosciences 4, 545–558.
Ellery, A., Wynn-Williams, D., 2003. Why Raman spectroscopy on Mars? – a case of the right tool for the right job. Astrobiology 3 (3), 565–579.
de Faria, D.L.A., Silva, S.V., Oliveira, M.T. de, 1997. Raman microspectroscopy of some iron oxides and oxyhydroxides. J. Raman Spectrosc. 28 (February), 873–878.
Fraeman, A.A., et al., 2013. A hematite-bearing layer in Gale Crater, Mars: mapping and implications for past aqueous conditions. Geology 41, 1103–1106.
Griffiths, A., et al., 2006. Context for the ESA ExoMars rover: the Panoramic Camera (Pancam) instrument. Int. J. Astrobiol. 5, 269–275.
Hartman, H., McKay, C.P., 1995. Oxygenic photosynthesis and the oxidation state of Mars. Planet. Space Sci. 43 (1-2), 123–128.
Haskin, L.A., et al., 1997. Raman spectroscopy for mineral identification and quantificafion for in situ planetary surface analysis: a point count method. J. Geophys. Res. 102 (97), 19293–19306.
Hurowitz, J.A., et al., 2010. Origin of acidic surface waters and the evolution of atmospheric chemistry on early Mars. Nat. Geosci. 3 (5), 323–326.
Marshall, C.P., Olcott Marshall, A., 2013. Raman hyperspectral imaging of micro-fossils: potential pitfalls. Astrobiology 13 (10), 920–931.
Morris, R.V., et al., 2000. Mineralogy, composition, and alteration of Mars Pathfinder rocks and soils: evidence from multispectral, elemental, and magnetic data on terrestrial analogue, SNC meteorite, and Pathfinder samples. J. Geophys. Res. 105, 1757.
Morris, R.V., Golden, D.C., Bell, J.F., 1997. Low-temperature reflectivity spectra of red hematite and the color of Mars. J. Geophys. Res. 102, 9125.
Mykura, W., 1960. The replacement of coal by limestone and the reddening of coal measures in the Ayrshire coalfield. Bull. Geol. Surv. GB 16, 69–109.
Parnell, J., et al., 2013. Detection of reduced carbon in a basalt analogue for martian nakhlite: a signpost to habitat on Mars. Int. J. Astrobiol. 13 (02), 124–131.
Pavlov, A.K., et al., 2013. Influence of cosmic rays on biomarkers on the Mars. Bull. Russ. Acad. Sci.: Phys. 77 (5), 596–598.
Pérez, F.R., Martinez-Frias, J., 2006. Raman spectroscopy goes to Mars. Spectrosc. Eur. 18 (1), 18–21.
Schuerger, A.C., et al., 2006. Rapid inactivation of seven Bacillus spp. under simulated Mars UV irradiation. Icarus 181, 52–62.
ten Kate, I.L., et al., 2005. Amino acid photostability on the Martian surface. Meteorit. Planet. Sci. 40 (8), 1185.
Tarling, D.H., et al., 1976. Palaeomagnetic dating of haematite genesis in Orcadian Basin sediments. Scott. J. Geol. 12 (2), 125–134.
Tuinstra, F., Koenig, J.L., 1970. Raman Spectrum of graphite. J. Chem. Phys. 53 (3), 1126.
Vago, J., et al., 2006. ExoMars – searching for life on the Red planet. ESA Bull.-Eur. Space Agency 126, 16–23.
Wang, A., Haskin, L.A., Cortez, E., 1998. Prototype Raman spectroscopic sensor for in situ mineral characterization on planetary surfaces. Appl. Spectrosc. 52 (4), 477–487.
Wang, W.H., 1992. Origin of reddening and secondary porosity in Carboniferous sandstones, Northern Ireland. Geol. Soc. Lond. Spec. Publ. 62, 243–254.
Wopenka, B., Pasteris, J.D.P., 1993. Structural characterization of kerogens to granulite-facies graphite: applicability of Raman microprobe spectroscopy. Am. Mineral. 78, 533–557.
Zent, P., 1998. On the thickness of the oxidized layer of the Martian regolith. J. Geophys. Res. 103 (98), 31 491–31,498.